Electronic Supplementary Material (ESI) for RSC Advances.

Supporting Information

Targeted Delivery of Bromelain using Dual Mode Nanoparticles: Synthesis, Physico-chemical Characterization, *in Vitro* and *in Vivo* Evaluation

Authors: Rozita Nasiri[1], Javad Hamzehalipour Almaki[1], Ani Idris*[1], Mahtab Nasiri[2], Muhammad Irfan[1], Fadzilah Adibah Abdul Majid[3], Hamid Rashidi Nodeh[4], Rosnani Hasham[5]

[1] Institute of Bioproduct Development, Department of Bioprocess Engineering, Faculty of Chemical and Energy Engineering, Universiti Teknologi Malaysia, Skudai 81110, Johor Bahru, Johor, Malaysia.
[2]Advanced Materials Research Centre, Department of Materials Engineering, Islamic Azad University, Najafabad Branch, Najafabad, Iran.
[3]Institute of Marine Biotechnology, Universiti Malaysia Terengganu, Kuala Terengganu, Malaysia.
[4]Department of Analytical Chemistry, University of Tehran, Tehran, Iran.
[5]Institute of Bioproduct Development, Universiti Teknologi Malaysia, Skudai 81110, Johor Bahru, Johor, Malaysia.

***E-Mail:** ani@cheme.utm.my ; rozfish4524@gmail.com

Figure S1 depicts characterization and physico-chemical analyses of synthesized nanoparticles through some methods such as FT-IR, TGA, DLS, XRD and microscopic observation of SPIONs-Br-FA in the absence of the magnetic field.

The FT-IR spectra of the bare SPIONs, SPIONs-COOH, SPIONs-Br and SPIONs-Br-FA are shown in figure S1 (A). For the analysis of the functional groups exposed on the surface of the SPIONs, FT-IR spectroscopy was performed in the wavenumber range of 4000-400 cm^{-1}. The FT-IR spectra of SPIONs and SPIONs-COOH also had been reported in our previous published paper as well [1]. Peaks centered at 582 cm^{-1} (Figure S1 A (a)) which were related to the lattice absorption of γ-Fe_2O_3 for the absorption bond of Fe–O characterized the presence of maghemite whereby the existence of initially synthesized SPIONs (γ-Fe_2O_3) was confirmed [2]. The treatment of the SPIONs with CA introduced carboxylic functional group on the surface of nanoparticles. As shown in figure S1 (A), the absorption peaks around 1623 cm^{-1} and 1400 cm^{-1} (Figure S1 A (b)) clearly show the presence functional -COOH group on nanoparticles surface [3], [4]. The absorption band at 1623 cm^{-1} is attributed to the generated carbonyl vibration (C=O, symmetric stretching) surface of nanoparticles [4]. In addition, the existence of bromelain in SPIONs-Br was confirmed through the comparison of FT-IR peaks before and after Br conjugation. Compared to SPIONs-COOH, spectrum of SPIONs-Br shows new extra absorption peaks. Over the course of the conjugation process through EDC/NHS method, the -COOH functional group on the SPIONs-COOH was activated so that it could covalently attach to the -NH_2 of the Br to form CO-NH band. As it is seen in Figure S1 A (c), the peaks about ~1688 and ~1490 cm^{-1} assigned for amide I (C-O stretching) and amide II bands (N-H bending) of conjugates, respectively; it is probably because of the formation of CO-NH by conjugation [5]. Also the fingerprint absorption band of maghemite (~581 cm^{-1}) is observed for the conjugates (Figure S1 A (c)), which shows that Br has been successfully conjugated to the SPIONs-COOH [5]. The bands around 3800, 3745 and 3412 cm^{-1} (Figure S1 A (c)) are assigned to the stretch of the N-H bonds in the Br. O-H vibrations from the water molecules which are trapped in the SPIONs-Br could also be represented by this band [6]. The presence of the stretching band C-N at 1070 cm^{-1} (Figure S1 A (c)) was a remarkable fact confirming the covalent conjugation via amide linkage [7], [8]. As it is seen in Figure S1 A (d), there is no strong proof of FA binding through FT-IR spectra due to overlapped bonding, but the amide II band (N-H bending, ~1490 cm^{-1}) of the FA conjugates are much stronger than those of SPIONs-Br indicating its presence.

Curves obtained from TGA analyses of naked SPIONs, SPIONs-COOH, SPIONs-Br and SPIONs-Br-FA are shown in figure S1 (B). A weight loss of almost 9.6% was recorded for the naked SPIONs throughout the whole temperature range, which might be due to water evaporation. Due to the removal of absorbed chemical and physical water, weight loss of SPIONs-COOH is minor (9%) below 200° C while the weight loss of about 13% from 250° C to 550° C can be associated with the removal of attached carboxyl group from the surface of SPIONs-COOH [9], [10], [11]. Between 600 to 800° C, no significant weight change was recorded, representing the existence of only SPIONs. For SPIONs-Br, significant weight loss (53%) occurred from 200 to 700° C. The weight percentage of conjugated Br on SPIONs-Br was calculated to be about 30% [12]. The SPIONs-Br shows 70% weight loss started from 250° C and it gradually continue till 750° C , which is related to CA, Br and FA decomposition respectively. The weight percentage of conjugated FA on SPIONs-FA was calculated to be about 17%. Results illustrate ~ 30 wt% magnetic content of the functionalized SPIONs.

Using DLS measurements, polydispersity index (PDI) of 0.278 ± 0.059 was obtained which illustrated that SPIONs-Br-FA was stable and narrowly distributed in solution. Normally, DLS measures a greater size since it detects the particle hydrodynamic diameter which includes the solvation layers. Therefore, the difference between the sizes measured by TEM and DLS is probably not related to the aggregation of the nanoparticles in solution. The hydrodynamic diameter and polydispersity index of nanoparticles in each step are presented in figure S1 ((C) and (D)). Compared to the SPIONs-COOH (60.088 nm), the hydrodynamic size distribution of Br and FA-conjugated nanoparticles significantly increased which indicated that the size distributions became broader after Br and FA conjugation. In terms of stability, the hydrodynamic size of final engineered SPIONs-Br-FA did not have significant changes within 3 month compared to the control group at 0 month (Figure S1 ((C) and (D)).

The size of a practical delivery system lies between 10–150 nm. Delivery systems are spleen-separated and renally sequestered if possessing sizes greater than 200 nm or less than 10 nm, respectively [13], [14]. As a proper candidate for biomedical applications, the final size of the SPIONs-Br-FA was in the practical range. The zeta potential of the prepared SPIONs-Br-FA was highly negative -19.78 Mv, which is attributed to the presence of free carboxylic groups in the structure of conjugated FA. The surface charges of the SPIONs, SPIONs-COOH,

SPIONs-Br and SPIONs-Br-FA at physiological pH 7.4 were measured as +15.46, -32.94, -20.10 and -19.78 Mv, respectively.

Via XRD, the evaluation of the composition and phase purity of the SPIONs and SPIONs-COOH were carried out. Figure S1 ((G) and (H)) illustrates the existence of diffraction peaks of γ-Fe_2O_3 nanoparticles (JCPDS file no. 00-004-0755) at 2θ = 30.1, 35.5, 43.2, 53.6, 57.1, 62.7 and 74.2° corresponding to the planes (220), (311), (400), (422), (511), (440) and (533); thus indicating the phase obtained was of γ-Fe_2O_3. There were no changes the crystalline structure of nanoparticles after the CA modification (Figure S1 (H)), but the intensity decreased. The XRD pattern of SPIONs-COOH showed similar pattern obtained elsewhere [15]. The average crystallite sizes were calculated from the X-ray patterns using Scherrer's equation assuming a uniform distribution of particles. This equation involves the line broadening measurements (FWHM) of the most intense peak. Calculation of crystallite size through the Debye–Scherrer formula resulted in obtaining the sizes 8.5 and 12.8 nm, for SPIONs and SPIONs-COOH respectively.

Using AAS at 248.3 nm, the total iron contents of the samples were gauged and reported. The total iron content of SPIONs, SPIONs-COOH, SPIONs-Br and SPIONs-Br-FA were 19.98 g/l, 14.32 g/l, 7.34 g/l and 6.85 g/l respectively. The total iron content of SPIONs and SPIONs-COOH also had been reported in our previous published paper as well [1]. In order to observe magnetorheological (MR) behaviour of the SPIONs-Br-FA, the microscopical observation in the absence as well as in the presence of the magnetic field was performed. When the magnetic field was absent, random dispersion of the particles was obviously seen figure S1 (E). Although, figure S1 (F) shows thin structures of SPIONs-Br-FA in the presence of magnetic plates which were aligned in the direction of the external field.

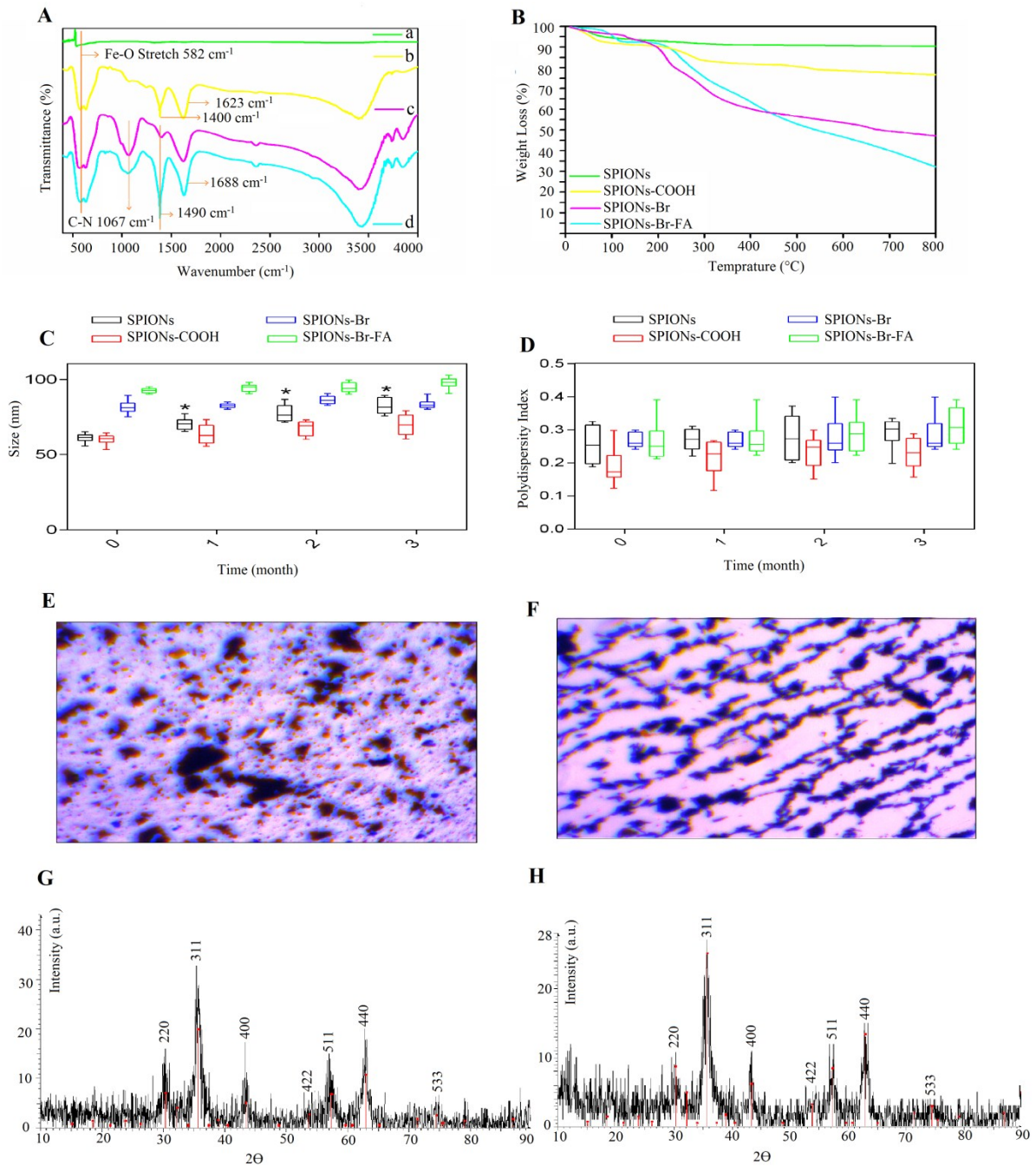

Figure S1 A) FT-IR spectra of synthesized and functionalized nanoparticles including (a) bare SPIONs, (b) SPIONs-COOH, (c) SPIONs-Br and (d) SPIONs-Br-FA, B) TGA curves of synthesized nanoparticles, C) The stability characteristics of SPIONs, SPIONs-COOH, SPIONs-Br and SPIONs-Br-FA in terms of mean hydrodynamic diameter (nm), D) Polydispersity index (PDI) of synthesized nanoparticles, E) Microscopic observation of the SPIONs-Br-FA in the absence of the magnetic field, F) Microscopic observation of the SPIONs in the presence of the magnetic field, G) XRD patterns of non-coated SPIONs and H) XRD patterns of coated SPIONs.

Blood has antithrombotic and anticoagulant properties through which it contacts the interior surface of blood vessels (endothelium). Both SPIONs and SPIONs-COOH are considered as foreign materials due to lack of endothelium function that complements the formation of thrombus resulting in fibrin matrix. High level of biocompatibility is addressed by the late formation of fibrin and highly accelerated conversion of fibrinogen into insoluble fibrin is addressed by quick blood clotting. The clotting factor is affected while the chemistry of blood is disturbed while in contact with the poor biocompatible substances. Therefore, to judge how the samples affect the chemistry of the blood, a key parameter is to study the coagulation factor. In order to determine the biocompatibility of synthesized nanoparticles the coagulation factors assay including APTT, PT, TT, FB and haemolysis tests were performed. The following test was carried out to indicate the biocompatibility level of SPIONs-COOH compared to bare SPIONs. In terms of clotting time (at concentrations 100, 200 and 300 μg/ml of nanoparticles), the SPIONs-COOH exhibited higher clotting time compare to the bare SPIONs for all APTT tests (Figure S2 (e)), PT (Figure S2 (a)), TT (Figure S2 (b)), FB (Figure S2 (c)) and hard clotting (Figure S2 (f)) tests compared to the bare SPIONs. FB formation concentration was lower for SPIONs-COOH compare to the bare SPIONs at same concentration (Figure S2 (d)). However the FB concentration for bare SPIONs was higher than that for SPIONs-COOH, it is still within acceptable range. Through the coagulation factors assay, it was concluded that the SPIONs-COOH is more compatible than bare SPIONs proven by the increasing the APTT, PT, TT and FB time and decreasing FB formation in concentrations < 300 μg/ml.

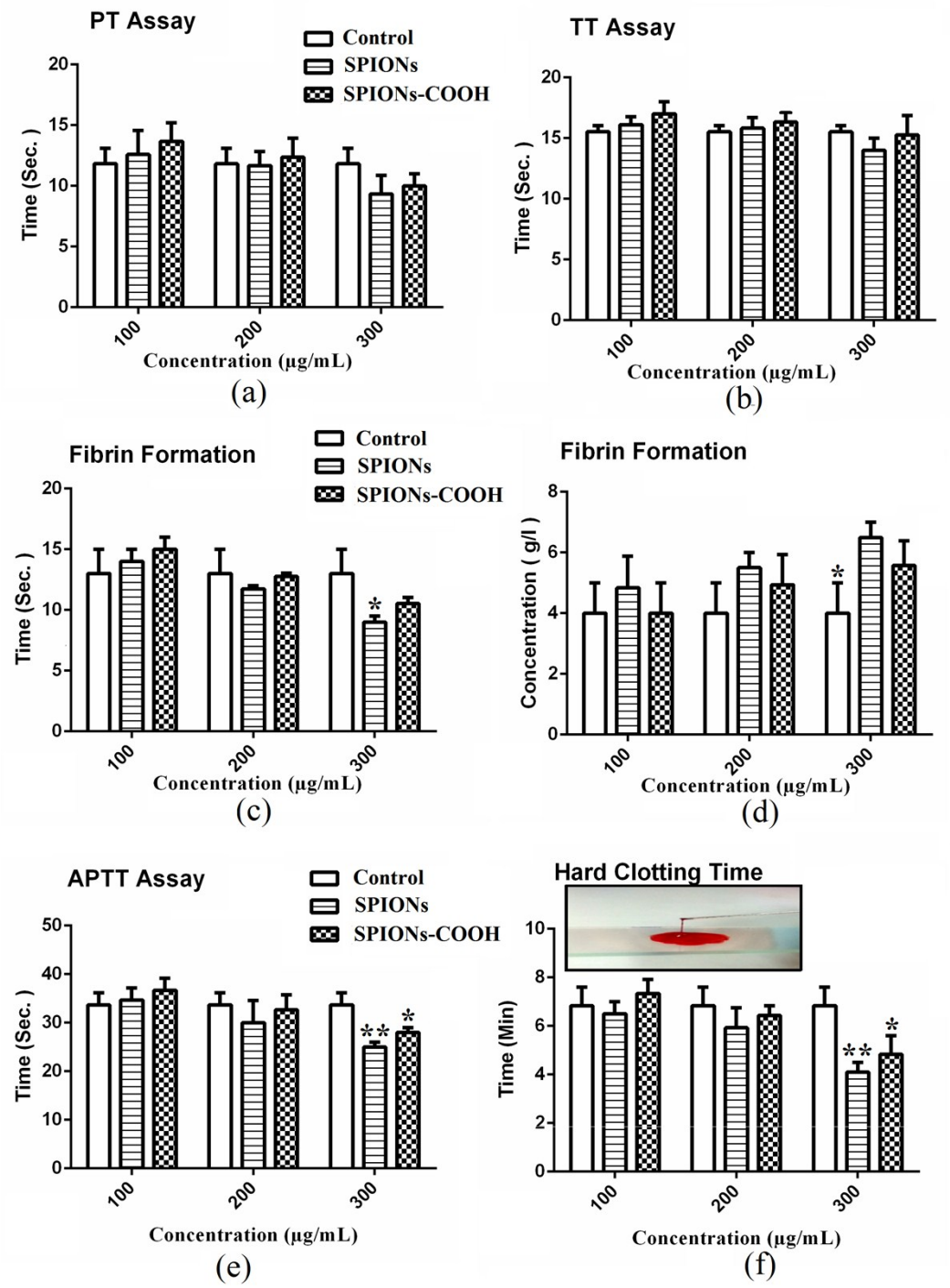

Figure S2 Coagulation factors assay and hard clotting time test after blood incubation with different concentrations of nanoparticles. a) PT assay, b) TT assay, c) FB/Time assay, d) FB/Concentration assay, e) APTT assay and f) Hard clotting time assay, (* $P < 0.05$) and (** $P < 0.01$) indicate significant differences compared to the control analyzed by one-way ANOVA.

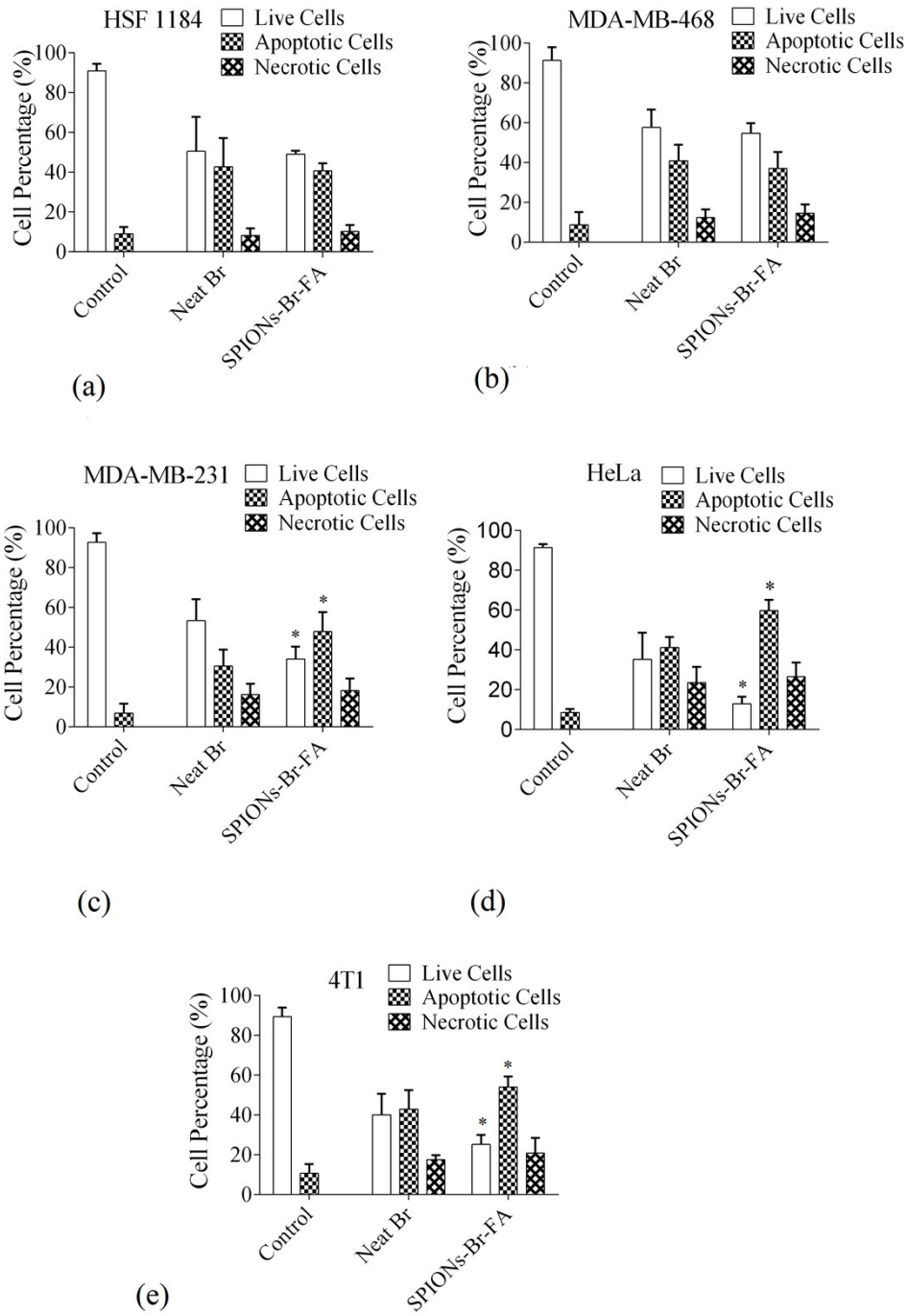

Figure S3 Percentages of live, apoptotic, and necrotic cells at different cell lines treated with neat Br and SPIONs-Br-FA. Frequencies of apoptotic cells treated with SPIONs-Br-FA was higher compare to neat Br. Data is represented as means ± SEM. of three replicates in three independent experiments, counting a minimum of 200 total cells each. (*) indicates a statistically significant difference from their respective vehicle control (one way ANOVA, $P < 0.05$).

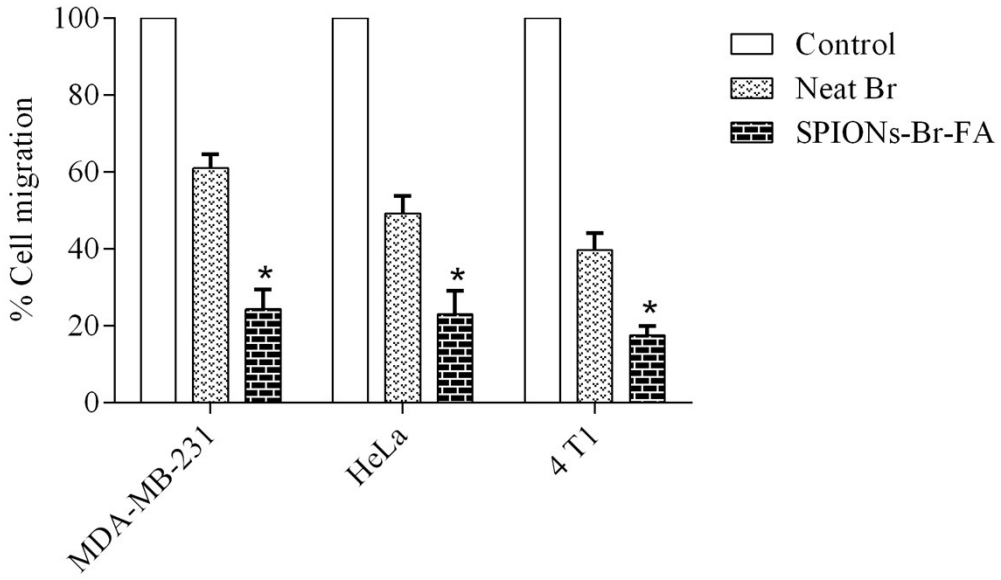

Figure S4 Quantitative analysis of migration inhibition rate of neat Br and SPIONs-Br-FA. Closure rate of scratches were examined quantitatively as the difference between scratch width at 24 h and outcomes were expressed as percentage of cell migration. Data are represented as means ± S.E.M. of three replicates in three independent tests. (*) indicates significant difference between SPIONs-Br-FA-treated and the neat Br-treated cells analyzed via unpaired t-test followed by Holm-Sidak post hoc test ($p < 0.05$).

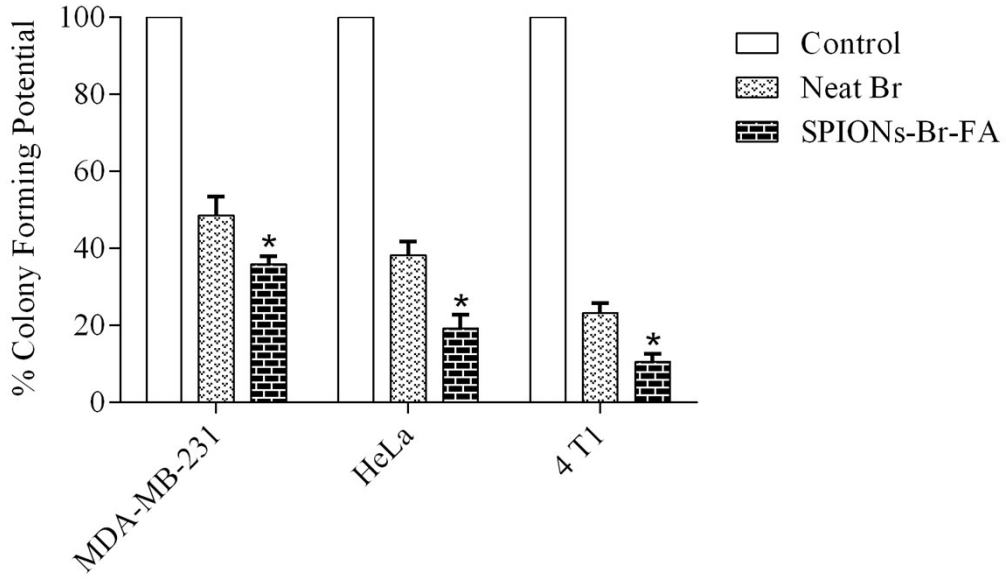

Figure S5 Inhibition potential of colony forming (quantitative analysis). Using an inverted microscope, the number of colonies was counted. The cell clonogenicity is reported as percent of control at each dose of extract. Results are shown as means ± S.E.M. of three replicates in three independent experiments. (*) indicates significant difference between SPIONs-Br-FA-treated and the neat Br-treated cells analyzed using unpaired t-test followed by Holm-Sidak post hoc test ($p < 0.05$).

Figure S6 represents the qualitative biodistribution of SPIONs-FA in 4 T1 bearing mice model using TEM staining method. The black spots (in TEM images) show the biodistribution of SPIONs-FA inside the vital organs. These observations confirmed the qualitative analysis (by AAS) results where SPIONs-FA accumulated in liver and spleen (RES system), kidney (due to the presence of FAR receptors in renal tissue and kidney) and tumor site.

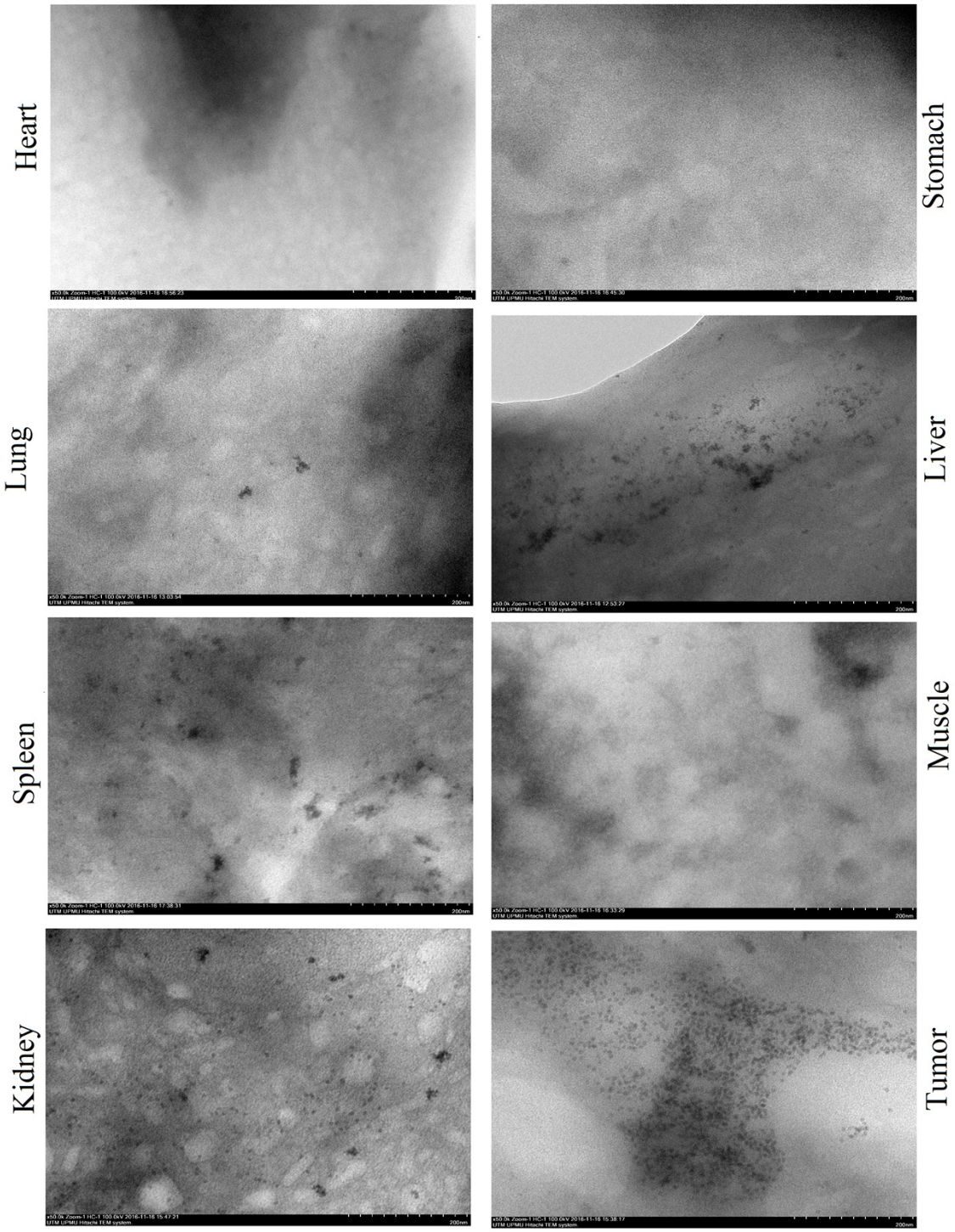

Figure S6 Qualitative biodistribution study (TEM staining) of vital organs (heart, lung, spleen, kidney, stomach, liver, muscle and tumor) 24 h after injection of SPIONs-FA (10 mg/kg) in tail vein of 4 T1 bearing mice model.

References

[1] R. Nasiri, J.H. Almaki, A.B. Idris, F.A.A. Majid, M. Nasiri, M. Salouti, M. Irfan, N. Amini, M. Marvibaigi, In vitro evaluation of actively targetable superparamagnetic nanoparticles to the folate receptor positive cancer cells, Mater. Sci. Eng. C. 69 (2016) 1147–1158.

[2] J.H. Almaki, R. Nasiri, A. Idris, F.A.A. Majid, M. Salouti, T.S. Wong, S. Dabagh, M. Marvibaigi, N. Amini, Synthesis, characterization and *in vitro* evaluation of exquisite targeting SPIONs–PEG–HER in HER2+ human breast cancer cells, Nanotechnology. 27 (2016) 105601. doi:10.1088/0957-4484/27/10/105601.

[3] S. Nigam, K.C. Barick, D. Bahadur, Development of citrate-stabilized Fe 3 O 4 nanoparticles : Conjugation and release of doxorubicin for therapeutic applications, J. Magn. Magn. Mater. 323 (2010) 237–243. doi:10.1016/j.jmmm.2010.09.009.

[4] A. Airinei, Citric-acid – coated magnetite nanoparticles for biological applications, 121 (2006) 117–121. doi:10.1140/epje/i2006-10051-y.

[5] Z. Wang, C. Zhou, J. Xia, B. Via, Y. Xia, F. Zhang, Y. Li, L. Xia, Colloids and Surfaces B : Biointerfaces Fabrication and characterization of a triple functionalization of graphene oxide with Fe 3 O 4 , folic acid and doxorubicin as dual-targeted drug nanocarrier, Colloids Surfaces B Biointerfaces. 106 (2013) 60–65. doi:10.1016/j.colsurfb.2013.01.032.

[6] M. Kamal Ahmadi, M. Vossoughi, Immobilization of α-Chymotrypsin on the Surface of Magnetic/Gold Core/Shell Nanoparticles, J. Nanotechnol. 2013 (2013).

[7] G.A. Mansoori, K.S. Brandenburg, A. Shakeri-Zadeh, A comparative study of two folate-conjugated gold nanoparticles for cancer nanotechnology applications., Cancers (Basel). 2 (2010) 1911–28. doi:10.3390/cancers2041911.

[8] D.K. Bora, P. Deb, Fatty Acid Binding Domain Mediated Conjugation of Ultrafine Magnetic Nanoparticles with Albumin Protein., Nanoscale Res. Lett. 4 (2008) 138–143. doi:10.1007/s11671-008-9213-6.

[9] A.S. Lübbe, C. Alexiou, C. Bergemann, Clinical applications of magnetic drug targeting, J. Surg. Res. 95 (2001) 200–206.

[10] M.A.C. Stuart, W.T.S. Huck, J. Genzer, M. Müller, C. Ober, M. Stamm, G.B. Sukhorukov, I. Szleifer, V. V Tsukruk, M. Urban, Emerging applications of stimuli-responsive polymer materials, Nat. Mater. 9 (2010) 101–113.

[11] D. Schmaljohann, Thermo-and pH-responsive polymers in drug delivery, Adv. Drug Deliv. Rev. 58 (2006) 1655–1670.

[12] Y. Shen, Y. Zhang, X. Zhang, X. Zhou, X. Teng, M. Yan, H. Bi, Horseradish peroxidase-immobilized magnetic mesoporous silica nanoparticles as a potential candidate to eliminate intracellular reactive oxygen species, Nanoscale. 7 (2015) 2941–2950.

[13] F. Alexis, E. Pridgen, L.K. Molnar, O.C. Farokhzad, reviews Factors Affecting the Clearance and Biodistribution of Polymeric Nanoparticles, 5 (2008) 505–515.

[14] M. Longmire, P.L. Choyke, H. Kobayashi, Clearance properties of nano-sized particles and molecules as imaging agents: considerations and caveats, (2008).

[15] M. Machovský, M. Mrlík, T. Plachý, I. Kuřitka, V. Pavlínek, Z. Kožáková, T. Kitano, The enhanced magnetorheological performance of carbonyl iron suspensions using magnetic Fe 3 O 4/ZHS hybrid composite sheets, RSC Adv. 5 (2015) 19213–19219.